

ARTICLES

The ABRF-MIRG'02 Study: Assembly State, Thermodynamic, and Kinetic Analysis of an Enzyme/Inhibitor Interaction

**D. G. Myszka,^a Y. N. Abdiche,^a
F. Arisaka,^b O. Byron,^c
E. Eisenstein,^d P. Hensley,^e
J. A. Thomson,^f C. R. Lombardo,^g
F. Schwarz,^b W. Stafford,ⁱ and
M. L. Doyle^j**

^aUniversity of Utah, Salt Lake City, UT; ^bTokyo Institute of Technology, Yokohama, Japan; ^cUniversity of Glasgow, Glasgow, Scotland; ^dUniversity of Maryland Biotechnology Institute, Rockville, MD; ^ePfizer, Inc., Groton, CT; ^fPfizer, Inc., La Jolla, CA; ^gThe Burnham Institute, La Jolla, CA; ^hNational Institute of Standards and Technology, Gaithersburg, MD; ⁱBoston Biomedical Research Institute, Watertown, MA; ^jBristol-Myers Squibb, Princeton, NJ

ADDRESS CORRESPONDENCE AND REPRINT REQUESTS TO: D. G. Myszka, Center for Biomolecular Interaction Analysis, University of Utah School of Medicine, Room no. 4A417, 50 N. Medical Drive, Salt Lake City, Utah 84132 (phone: 801-585-5358; fax: 801-585-3015; e-mail: david.myszka@cores.utah.edu),

The study was funded, in part, by the U.S. Department of Defense DARPA (F30602-00-2-0609).

DISCLAIMER: Certain commercial materials, instruments, and equipment are identified in this manuscript in order to specify the experimental procedure as completely as possible. In no case does such identification imply a recommendation or endorsement by NIST nor does it imply that the materials, instruments, or equipment identified are necessarily the best available for the purpose.

Fully characterizing the interactions involving biomolecules requires information on the assembly state, affinity, kinetics, and thermodynamics associated with complex formation. The analytical technologies often used to measure biomolecular interactions include analytical ultracentrifugation (AUC), isothermal titration calorimetry (ITC), and surface plasmon resonance (SPR). In order to evaluate the capabilities of core facilities to implement these technologies, the Association of Biomolecular Resource Facilities (ABRF) Molecular Interactions Research Group (MIRG) developed a standardized model system and distributed it to a panel of AUC, ITC, and SPR operators. The model system was composed of a well-characterized enzyme-inhibitor pair, namely bovine carbonic anhydrase II (CA II) and 4-carboxybenzenesulfonamide (CBS). Study participants were asked to measure one or more of the following: (1) the molecular mass, homogeneity, and assembly state of CA II by AUC; (2) the affinity and thermodynamics for complex formation by ITC; and (3) the affinity and kinetics of complex formation by SPR. The results from this study provide a benchmark for comparing the capabilities of individual laboratories and for defining the utility of the different instrumentation.

KEY WORDS: Plasmon, calorimetry, ultracentrifugation, kinetics, affinity.

Characterizing noncovalent interactions between molecules is central to our understanding of biomolecular and cellular function, and to the discovery and development of medicines. However, measuring molecular-level binding parameters that are both precise and accurate is a challenge that requires specialized training and equipment. Given their general utility, we often find that the expertise and equipment to perform molecular interaction analysis resides in core facilities. The Association of Biomolecular Resource Facilities (ABRF) established the Molecular Interactions Research Group (MIRG) to advance the state-of-the-art application of molecular interaction analysis in these facilities. Three of the most widely used and complementary technologies

for characterizing biomolecular interactions are analytical ultracentrifugation (AUC), isothermal titration calorimetry (ITC), and surface plasmon resonance (SPR). Together, these tools provide a highly resolved definition of macromolecular interactions in terms of the assembly state, thermodynamics, affinity, and kinetics of complex formation.

We report on a study conducted by MIRG to evaluate the capabilities of independent groups to implement AUC, ITC, and SPR. A well-characterized enzyme-inhibitor pair, namely bovine carbonic anhydrase II (CA II) and 4-carboxybenzenesulfonamide (CBS), was adopted as a standard model system because the reactants were commercially available, inexpensive, nonhazardous, and amenable to AUC, ITC, and SPR analysis in a standard aqueous buffer system at room temperature. Another advantage was that the X-ray crystal structures of CA II complexes with various aryl sulfonamides revealed a single stoichiometric binding site per enzyme molecule. The model system was distributed to a panel of AUC, ITC, and SPR operators who were asked to measure one or more of the following: (1) molecular mass, homogeneity, and assembly state by AUC, using equilibrium and velocity approaches, (2) affinity and apparent binding enthalpy change by ITC, and (3) the affinity and kinetics of complex formation by SPR. The results from this study provide a benchmark for comparing the capabilities of individual laboratories and for defining the utility and corroborative use of these complementary technologies.

METHODS

Participants of the MIRG'02 study were sought through communications at ABRF meetings, the ABRF web site, e-mail to members of Reversible Associations in Structural and Molecular Biology, and word of mouth. Participants were supplied with reagents and experimental guidelines for each technology that they volunteered to use. CA II (30 kg mol^{-1}) from bovine erythrocytes was purchased as a lyophilized powder of 88% mol purity (product no. C2522) from Sigma-Aldrich (St. Louis, MO). CBS (201.2 g mol^{-1}) was purchased as a 97% mol pure powder (product no. 108420050) from Acros Organics (Morris Plains, NJ). Both reagents were used without further purification. They were either dispensed into aliquots and stored in plastic Eppendorf tubes at -80°C or dissolved in $0.020 \text{ mol L}^{-1} \text{ Na}_2\text{HPO}_4\text{-NaH}_2\text{PO}_4$ and $0.150 \text{ mol L}^{-1} \text{ NaCl}$ at $\text{pH} = 7.4$ buffer (PBS) which was prepared according to a standard protocol that was supplied to all study participants. Briefly, the method involved dissolving the monobasic (NaH_2PO_4) and dibasic

(Na_2HPO_4) forms of sodium phosphate in water to give 0.2 mol L^{-1} stock solutions, with respective pH values of ~ 5.2 and ~ 9.3 . The two stock solutions were mixed together in a 1:4 v/v ratio to give $\text{pH} \sim 7.4$. Fine pH adjustments were made using concentrated solutions of either NaOH or HCl dropwise, as appropriate. The solution was diluted 10-fold in water and sodium chloride was added to a final concentration of 0.150 mol L^{-1} . Buffers were filtered ($0.2 \mu\text{m}$) and degassed prior to use. Prior to distributing the reagents, formulation and stability studies showed that they were stable for several weeks at 4°C with respect to activity and aggregation and could be shipped at ambient temperature. Participating groups were identified by codes to maintain their anonymity.

AUC Analysis

AUC participants reconstituted CA II to 2 mg mL^{-1} in the PBS buffer and dialyzed the solution exhaustively against the same buffer. Values for the theoretical molecular weight of CA II ($28,981 \text{ g mol}^{-1}$), its extinction coefficient at $\lambda = 280 \text{ nm}$ ($\epsilon_{280 \text{ nm}} = 50,070 \text{ L mol}^{-1} \text{ cm}^{-1}$) and its partial specific volume (0.736 ccm g^{-1}) were provided. The latter was computed from the amino acid sequence for CA II (Swissprot locus CAH2_Bovin accession P00921) using a consensus volumes method.¹ Assays were conducted at 20°C .

Sedimentation Equilibrium

Participants chose one of two 12-mm cell formats, either a three-cell unit equipped with a standard double-sector centerpiece, or a single-cell equipped with an external loading six-channel Yphantis-type centerpiece (Beckman Part numbers: #366755 for the centerpiece and #368115 for the housing). The latter was advantageous for interference optics because optical blank runs were performed without dismantling the cells. The use of scrupulously clean, dry centerpieces prevented contamination. To quantitatively characterize the assembly state of native CA II in solution, samples were monitored at three different loading concentrations and rotor speeds and analyzed globally. Recommended speeds were 24,000, 28,000, and 34,000 rpm for sigma values of about 2.0, 2.8, and 4.0 cm^{-2} . Sigma is defined in Equation 1 and represents the protein's reduced monomer molecular weight.²

$$\sigma \equiv \frac{\omega^2 s}{D} = \frac{M(1-\nu\rho)\omega^2}{RT} = \frac{d \ln c}{d(r^2/2)} \quad (\text{Eq. 1})$$

where ω is the angular velocity, s is the sedimentation coefficient, D is the translational diffusion coefficient,

M is the molecular weight, ν is the partial specific volume, ρ is the solution density, R is the gas constant, T is the temperature in K, c is the solute concentration, and r is the radial distance from the center of rotation.

Absorbance Optics

CA II samples (0.125 mL) were loaded at concentrations that yielded optical densities of 0.9, 0.3 and 0.1 at $\lambda = 280$ nm. A preliminary blank run was recommended as a quality control, following the same protocol as that used for standard double-sector centerpieces with interference optics (described below). If the buffer absorbed appreciably, the menisci were matched more closely. Contrary to the manufacturer's suggested protocol, participants were cautioned against overfilling the reference side.

Interference Optics

Using standard double-sector centerpieces, a presample blank optic run was performed by adding 0.125 mL of water to reference and sample compartments. Several speeds were explored and blank images were recorded to correct subsequent sample scans for background optics. After the blank run, the screws were removed without dismantling the cell, which was then dried under vacuum. An equilibrium run was performed by adding buffer and sample to their respective compartments and matching their volumes (0.125 mL), as judged by inspecting their menisci, to enable proper buffer subtraction. This recommendation contradicted the manufacturer's literature. Using the six-channel external loading centerpieces, pre- and post-sample runs were performed. The CA II sample was measured at three loading concentrations of 1.0, 0.33, and 0.10 mg mL⁻¹.

Sedimentation Velocity

Velocity data were obtained by absorbance scans at $\lambda = 280$ nm using Beckman analytical ultracentrifuges. For absorbance optics, samples were measured in three cells at optical densities of 0.9, 0.3 and 0.1 using an extinction coefficient for CA II of $\epsilon_{280\text{ nm}} = 50,070$ L mol⁻¹ cm⁻¹. For interference optics, CA II was analyzed at four concentrations (typically 1.0, 0.3, 0.1, and 0.03 mg mL⁻¹) and at 50,000 rpm for 4 h. Scans were chosen from an appropriate range ($2.9 \times 10^{11} < \omega^2 t < 3.5 \times 10^{11}$) and sedimentation coefficient distributions were computed from the time derivative of the sedimentation velocity concentration profile using DCDT software that implemented algorithms described by Stafford.³ For participants using standard double-sector centerpieces, the protein solution (0.430

mL) was placed in the sample sector and an equal volume of dialysate was placed in the reference sector. For participants using capillary type synthetic-boundary centerpieces, the protein solution (0.420 mL) was placed in the sample sector and dialysate (0.440 mL) was placed in the reference sector. Synthetic-boundary centerpieces ensured that menisci were aligned properly, as demanded by high precision Rayleigh interference work at low protein concentrations. Under these conditions, it is important to minimize differential buffer redistribution during sedimentation. The procedure for synthetic-boundary and double-sector centerpieces differed by an extra step that was required to match the menisci. Precise cell alignment with the rotor scribe marks avoided convection in the sample that may foul the data.

Meniscus Matching When Using Synthetic-Boundary Centerpieces

After loading the rotors into their chamber, the vacuum was applied. When the pressure fell below 66.7 kPa, the rotor speed was increased to 3000 rpm, and the laser delay and window-timing parameters were set. Increasing the speed to 10,000 rpm for 30 s forced the menisci to match as judged by observing a single vertical meniscus line.

Laser Delay and Window Timing Parameters

For wide (standard) window holders, the parameter settings were as follows: (1) intensity $\sim 50\%$, (2) contrast ~ 110 , (3) window = 0.4 degrees, (4) delay was set to observe fringes, (5) angular distance between both sides of the sector was 1.4–1.6 degrees (corresponding to about ± 7 –8 clicks on the scroll arrows from the midpoint), (6) delay setting was adjusted by clicking until the image darkened and then clicking backward to set the delay to the center of the sector, (7) the picture was finely adjusted to contrast light and dark fringes equally. For superior reproducibility, interference windows were recommended. Adjustments were the same as above, except a window of 1.4 degrees was used to uniformly illuminate the slits and allow the slits to mask the region of the cell to be illuminated.

Data Analysis

AUC participants were invited to use their preferred data analysis methods in order to determine the molecular mass of the CA II sample. The chosen sedimentation velocity methods included the "time derivative and time difference methods" developed by Stafford,³ using either DCDT from the NAUF group or

DCDT+ from Philo,⁴ SEDANAL from Stafford (Stafford WF, personal communication, 2003), SEDFIT from Schuck and Rossmann,⁵ SVEDBERG using time difference data for the analysis of interference data from Philo,⁶ LAMM developed by Behlke and Ristau,⁷ and the VAN-HOLDE extrapolation method in software developed by Demeler and Saber.⁸

ITC Analysis

Lyophilized reagents were distributed to a panel of ITC users along with experimental guidelines. Titrations were performed at 25°C in PBS buffer. Study participants were instructed on how to reconstitute the CA II and how to dialyze against the assay buffer to prevent artifacts created by mismatched buffers. They were asked to determine the concentration of each reactant as follows. The CA II concentration was determined spectrophotometrically using an extinction coefficient computed from the amino acid sequence ($\epsilon_{280\text{ nm}} = 50,070\text{ L mol}^{-1}\text{ cm}^{-1}$), whereas the concentration of CBS was determined gravimetrically using a molecular mass of 201 g. Participants were also asked to measure the absorbance of the resulting CBS solution and were informed that the extinction coefficient of CBS fell between $\epsilon_{272\text{ nm}}$ values of 1000 and 1500 $\text{L mol}^{-1}\text{ cm}^{-1}$. ITC was used to determine the binding constant (K_A), molar binding ratio (N) and the binding enthalpy change (ΔH^{ITC}) of the CBS/CA II interaction. The recorded ΔH^{ITC} was uncorrected for possible proton-linked buffer heats of ionization. Participants were informed that the K_A of the interaction was within the range 5×10^5 to $3 \times 10^6\text{ L mol}^{-1}$ and that the CBS should be titrated from a syringe into a calorimeter cell containing CA II. Freedom was granted in other aspects of the assay design, such as the concentrations of reactants used in the titration, the injection schedule, the use of control titrations, and the data analysis method. Detailed information was requested from all study participants about the instrumentation and experimental parameters that they chose to employ.

SPR Analysis

The following method is intended for BIACORE 2000 and 3000 instruments and was adapted from the detailed protocol supplied to each SPR study participant. Operators of alternative platforms were asked to modify the method accordingly. SPR study participants received 75 μg CA II protein lyophilized from water and 0.6 mL of a solution containing 2 mmol L^{-1} CBS in PBS running buffer that was filtered (0.2 μm) and degassed prior to use.

Instrumentation and Materials

Interaction analysis was performed at 25°C using a range of SPR optical biosensors (BIACORE AB, Uppsala, Sweden and IASYS Affinity Sensors Ltd, Saxon Hill, Cambridge, UK) equipped with research grade CM5 sensor chips or equivalent solid supports. All data were collected at the highest rate available. Sensor chips and coupling reagents (N-ethyl-N'-dimethylaminopropylcarbodiimide, EDC; N-hydroxysuccinimide, NHS; and 1 M ethanolamine • HCl, pH 8.5) were purchased from BIACORE AB and Affinity Sensors Ltd.

Instrument Preparation

Desorb and preconditioning procedures were performed in water. An automated Desorb routine was conducted using reagents supplied by BIACORE (0.5% w/v SDS followed by 50 mmol L^{-1} glycine at pH 9.5). New, unmodified sensor surfaces were preconditioned at a flow rate of 100 $\mu\text{L min}^{-1}$ by treating them with a sequence of four reagents, each applied as two consecutive 12-s pulses: 50 mmol L^{-1} NaOH, 0.1% v/v HCl, 0.1% w/v SDS, and 0.085% v/v H_3PO_4 . Following three primes with freshly degassed PBS running buffer, the detector was normalized (automated procedure) with the appropriate concentration of glycerol to ensure maximum sensitivity. To test data quality and further equilibrate the fluidic system, a blank run was performed by injecting running buffer at a flow rate of 100 $\mu\text{L min}^{-1}$. Thirty cycles were performed using association and dissociation times of 1 and 3 min, respectively.

CA II Immobilization

Protein was immobilized at 10 $\mu\text{L min}^{-1}$ to create a high-capacity surface via a standard EDC/NHS-mediated amine coupling procedure.⁹ First, a freshly mixed aqueous solution containing 0.05 mol L^{-1} NHS in 0.2 mol L^{-1} EDC was injected for 7 min to activate a flow cell. Second, CA II was reconstituted to a concentration of 0.125 mg mL^{-1} in 10 mmol L^{-1} sodium acetate at pH 5.0 and injected for 10 min. Finally, a 7-min pulse of 1 mol L^{-1} ethanolamine at pH 8.5 was applied that deactivated excess activated ester groups. Unmodified flow cells served as reference and control surfaces.

Interaction Analysis

CBS was diluted threefold and serially into running buffer to final concentrations of 0.082, 0.25, 0.74, 2.22, 6.67, and 20.0 $\mu\text{mol L}^{-1}$. Each sample was dispensed into triplicate single-use, snap-capped plastic vials and randomized in the autosampler block, along with

samples containing only buffer. Ten *warm-up* buffer cycles began the run and were excluded from the analysis. Association and dissociation phases of all sample injections were monitored for 1 and 3 min, respectively, at a flow rate of 100 $\mu\text{L min}^{-1}$.

Data Processing

Response data as a function of time were processed as depicted in Figure 1. Typical raw data obtained for CBS injections across immobilized CA II are shown in Figure 1A. Y-averaging the response data to zero established a baseline response (Fig. 1B). Data were cropped (Fig. 1C) and the staggered injection start times (Fig. 1C, inset) were aligned so as to define a common start time for all injections at $t = 0$ s (Fig. 1D). Subtracting the responses generated across an unmodified reference surface (Fig. 1E, inset) referenced the data by correcting for bulk refractive index shifts and nonspecific binding to the dextran matrix (Fig. 1E). Subtracting an average buffer (or “blank”) response (Fig. 1F, inset) double referenced the data by removing systematic artifacts that occurred equally in

all sample injections (Fig. 1F).¹⁰ For the analysis described in Figure 8, every fifth injection provided the “blanks” for double referencing purposes.

Data Analysis

Fully processed CBS binding responses were analyzed globally by direct curve fitting to a simple bimolecular reaction mechanism ($A + B = AB$) using either BIAevaluation or CLAMP software,¹¹ which generated modeled data by numerical integration of the differential equations that described the binding mechanism. For each data set, an optimal set of kinetic rate constants (k_a and k_d) was calculated by least squares analysis. The ratio of the rate constants yielded values for the equilibrium dissociation constant, $K_D = k_d/k_a$. Each data set was allowed its own surface capacity, equivalent to an R_{max} value. The model converged upon an optimal set of injection times for all curves by floating the start times together and the stop times together. In addition, the refractive index increment for each measured curve was obtained by least squares analysis.

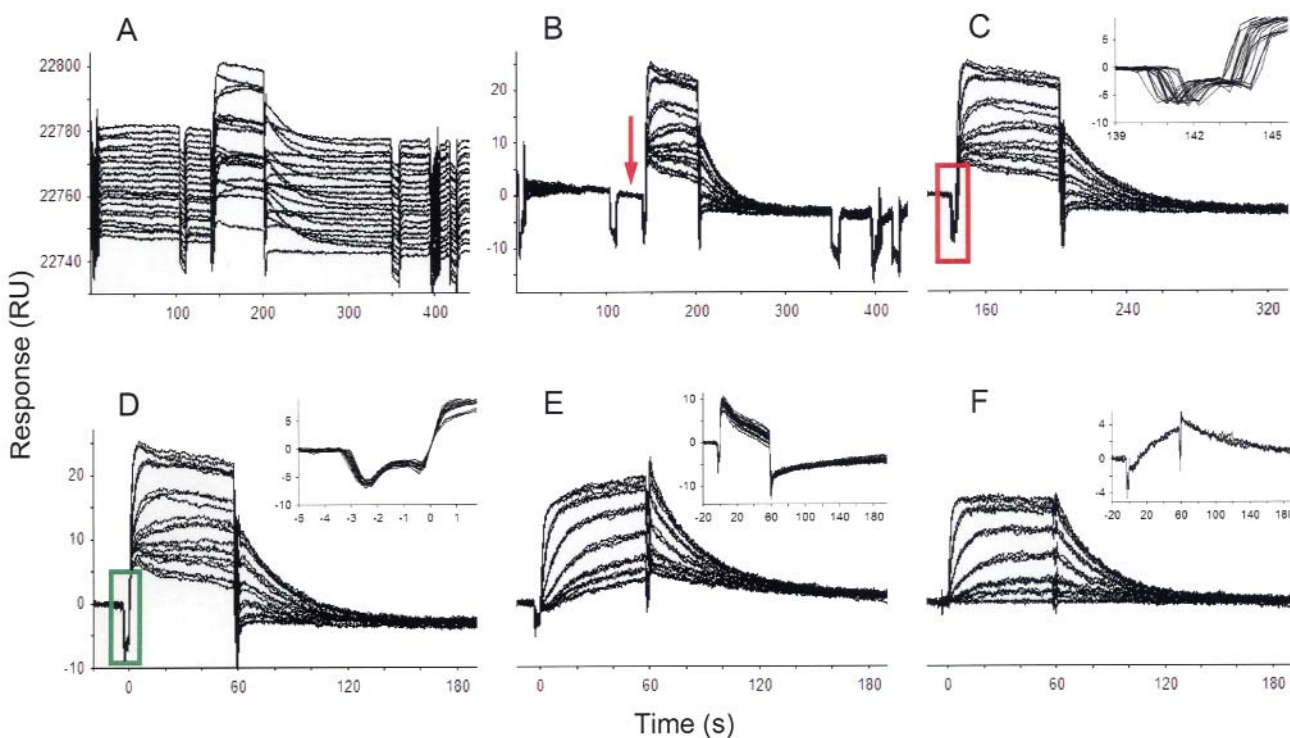


FIGURE 1

Processing SPR biosensor data. The example shows triplicate CBS binding responses collected across immobilized CA II. **A:** Raw data. **B:** Y-averaged to zero (red arrow). **C:** Cropped (inset: enlarged view of red box). **D:** X-aligned to zero (inset: enlarged view of green box). **E:** Referenced (inset: responses generated across an unmodified reference surface). **F:** Double referenced (inset: buffer responses).

van't Hoff Analysis

The CBS/CA II interaction was measured in a similar manner at 5, 15, 25, and 35°C. The equilibrium dissociation constants provided by the ratios of the kinetic rate constants determined at each temperature were used to obtain the van't Hoff enthalpy. A linear form ($Y = mX + c$) of the integrated van't Hoff equation was used to determine the $\Delta H_{\text{van't Hoff}}$ of the interaction ($\ln K_D = \Delta H_{\text{van't Hoff}}/RT - \Delta S/R$, where R is 1.987 cal mol⁻¹ K⁻¹ and T is in Kelvin). An approximate entropy change was computed from the Y-axis intercept, but a more reliable estimate was afforded by rearranging the Gibbs free energy change equation ($\Delta G^\circ = \Delta H_{\text{van't Hoff}} - T\Delta S$) and substituting values for $\Delta G^\circ = RT \ln K_D$ (298 K), $T = 298$ K, and $\Delta H_{\text{van't Hoff}}$.

RESULTS

AUC Analysis

The goal of the AUC portion of the MIRG study was to deduce the assembly state and the molecular mass of native CA II in solution at concentrations relevant to the ITC and SPR portions of the study. This information would aid in characterizing its interaction with CBS by ITC and SPR methods. Samples destined for AUC analysis were shipped to 13 groups, of which 5 completed the study. Participants handled the experiments with differing experimental strategies, combining the use of complementary sedimentation velocity and equi-

librium approaches with different data analysis programs. Multiple data sets were generated by each participant, spanning a range of sample concentrations and rotor speeds. Some participants reported globally derived parameters, while others reported parameters for individual experiments (see Table 1). Figure 2 depicts representative examples of the data obtained.

Sedimentation Equilibrium

Figures 2A and 2B show equilibrium concentration distributions of CA II samples monitored at a low rotor speed (24,000 rpm), where sedimentation and diffusion contributed equally to the distribution. Lower panels in Figures 2A and B show overlay plots of measured data (blue) and data that were simulated (red) to a single-exponential equation (Eq. 1) using nonlinear regression and assuming a single species. Upper panels in Figures 2A and B demonstrate the low and randomly scattered residuals for these data, demonstrating that the model closely described the data. Figure 3A shows the masses determined by two participants who each performed nine measurements. Within error there is no discernible change in the mass deduced for samples analyzed at different CA II concentrations (0.1, 0.3, 0.9 mg mL⁻¹) or rotor speeds (24,000, 28,000, and 34,000 rpm), consistent with a homogeneous solution of a monomer species. Figure 3B summarizes the equilibrium-based results reported by the five participants. Excluding the unexpectedly high value for participant 2, which is likely due to sample aggregation, the mean value for the remaining four participants ($29,000 \pm 1,000$ g mol⁻¹)

TABLE I

Summary of Sedimentation Velocity Results Analyzed by the LAMM Program as Reported by AUC Participant 1^a

[CA II] (mg mL ⁻¹)	λ (nm)	Subprogram ^b	$s_{20,W}$ (Svedbergs)	$D_{20,W}$ (Ficks)	$M_{s,D}$ (kg mol ⁻¹) ^c	f/f_0 ^d
0.70	292	WB	2.703 ± 0.001	8.83 ± 0.02	28.95 ± 0.08	1.172
0.70	292	M	2.692 ± 0.001	8.80 ± 0.02	28.92 ± 0.07	1.175
0.47	280	WB	2.718 ± 0.002	9.16 ± 0.02	28.19 ± 0.08	1.157
0.47	280	M	2.724 ± 0.001	9.13 ± 0.02	28.35 ± 0.07	1.159
0.28	235	WB	2.745 ± 0.001	8.80 ± 0.03	28.73 ± 0.10	1.167
0.28	235	M	2.734 ± 0.002	8.97 ± 0.03	28.79 ± 0.08	1.154

^aThe mean average mass ($M_{s,D}$) was deduced to be 28.7 ± 0.3 kg mol⁻¹.

^bWB indicates "whole boundary" analysis and M indicates "meniscus" analysis.

^c $M_{s,D}$ is calculated from the measured $s_{20,W}$ and $D_{20,W}$ values.

^dThe f/f_0 value is the ratio of the frictional coefficient of the molecule to that expected for a spherical molecule. It is a measure of the axial ratio and provides information on the shape of the molecule. The frictional coefficient f is calculated from the determined sedimentation coefficient and molecular weight, whereas f_0 is calculated from Stoke's law based on the molecular weight and assuming a spherical shape.

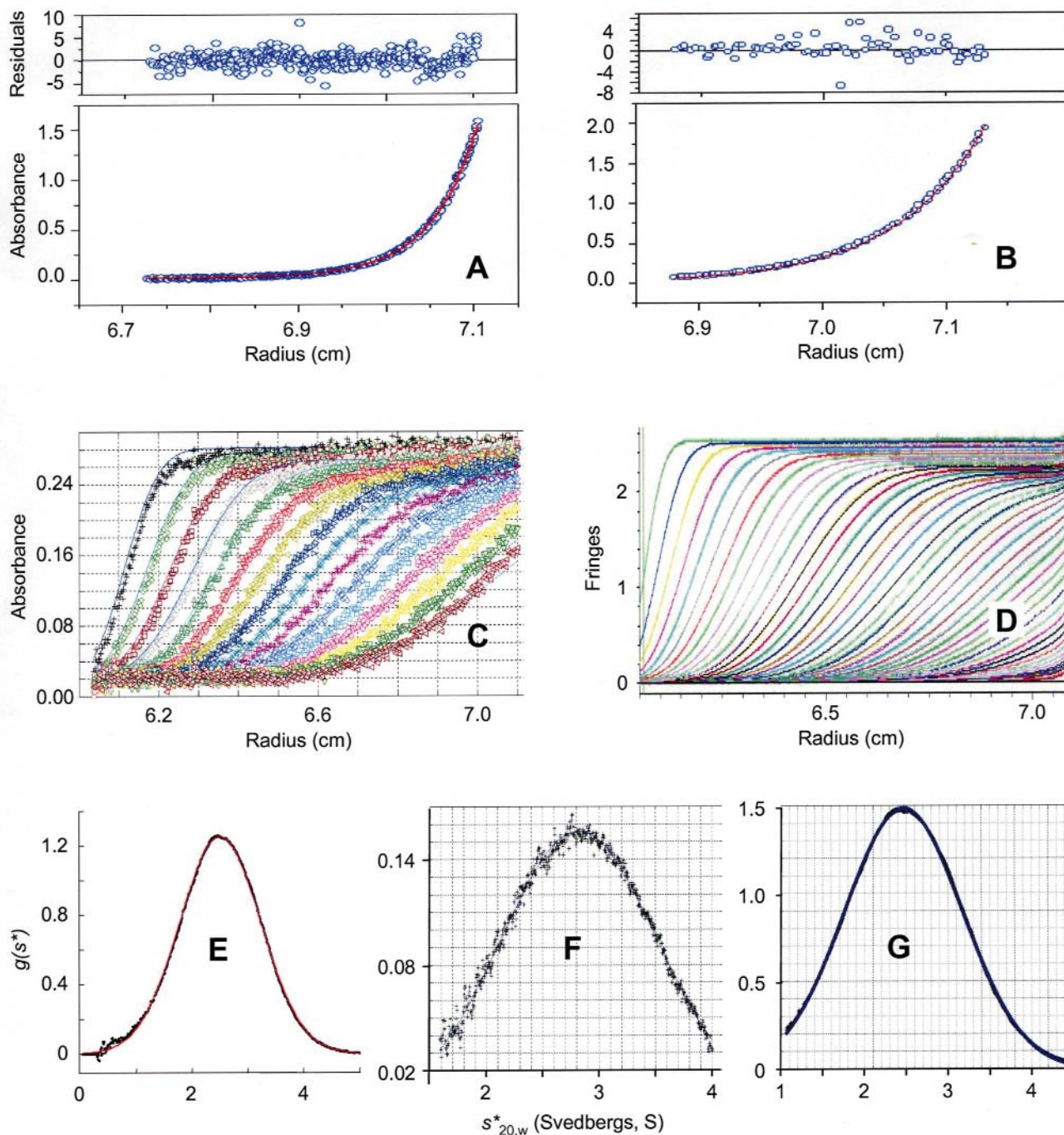
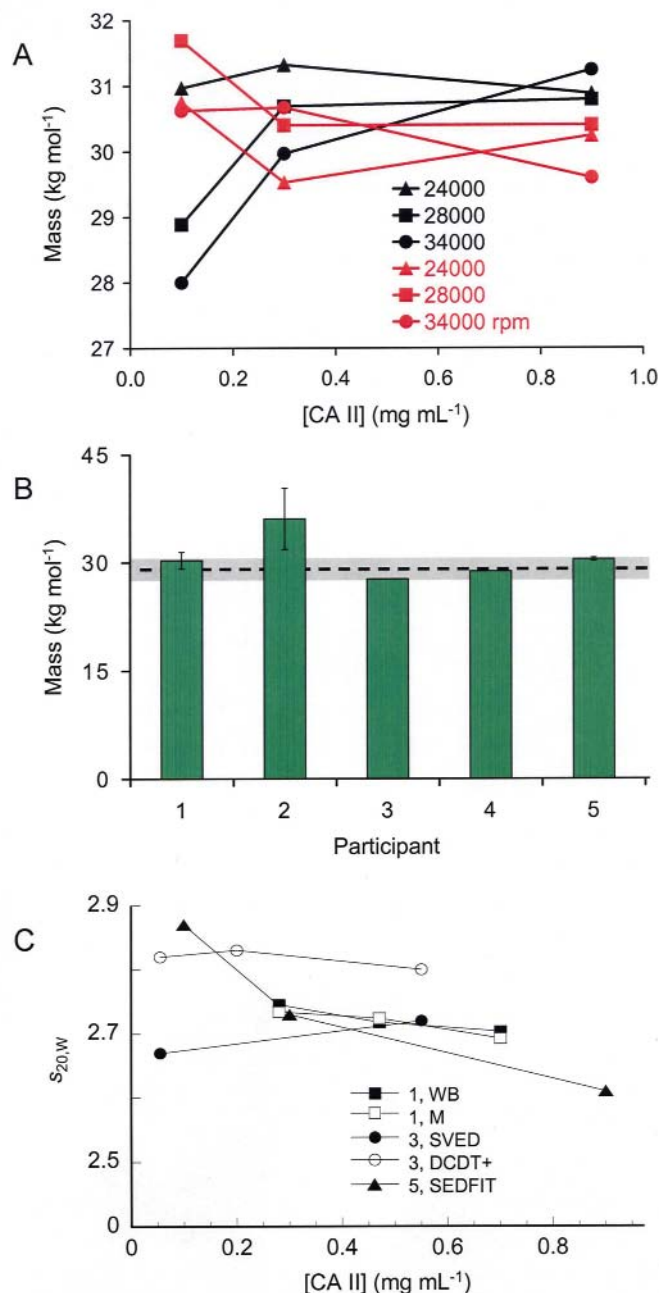


FIGURE 2

Representative data sets demonstrating the use of complementary equilibrium and velocity sedimentation approaches in the molecular mass determination of CA II. Panels **A** and **B** depict sedimentation equilibrium data, **C** and **D** depict velocity whole boundary analysis, and **E**, **F**, and **G** represent velocity time derivative analysis. For velocity measurements, the sedimentation coefficient (s) was computed using the Svedberg equation, where 1 Svedberg unit (S) = 0.1 picoseconds (or 1×10^{-13} s). Data shown in **C** were analyzed using approximate solutions of the Lamm equation, whereas data shown in **D** were analyzed by fitting $c(M)$ while floating f/f_0 .

**FIGURE 3**

Molecular masses determined by sedimentation equilibrium and velocity approaches. **A:** Examples of equilibrium-based mass determinations by participants 1 (black) and 5 (red) for CA II samples analyzed at three concentrations (0.1, 0.3, and 0.9 mg mL⁻¹) and at three rotor speeds: 24,000 (triangles), 28,000 (squares), and 34,000 rpm (circles).

B: Mean equilibrium-based masses obtained from five participants. Reported values for participants 1 and 5 each represent the mean of nine measurements (consistent with panel A), whereas a mean was derived for participant 2 from analyses performed at three different rotor speeds. Global best-fit values for data collected at various CA II concentrations and rotor speeds are shown for participants 3 and 4 (no standard errors were provided). The dotted line and gray band indicate the mean value obtained from four of the five participants (29 ± 1 kg mol⁻¹), excluding the outlying value provided by participant 2.

C: Velocity-derived sedimentation coefficients measured at various CA II loading concentrations by three participants (1, 3, and 5) using several data analysis methods. Participant 1 used the LAMM method with absorbance data and considered both the whole boundary (solid squares) and the meniscus condition (open squares). Participant 3 used Svedberg with absorbance data (solid circles) and DCDT+ with interference data (open circles). Participant 5 used Sedfit (solid triangles), and reportedly deconvoluted the data into three molecular weight species, of which only the main species is plotted here. Results submitted from participant 2 were excluded because they appeared to be outliers (mean $s_{20,w} = 3.68$). Participant 4 did not report velocity measurements.

agreed with the theoretical one based on the amino acid sequence (28,980 g mol⁻¹).

Boundary Sedimentation Velocity

Figures 2C and 2D show whole boundary scans detected by absorbance for CA II across a centrifuge cell rotating at a high speed (50,000 rpm). These data provided concentration profiles for CA II in the radial direction of time in response to the applied centrifugal force. Multiple scans spaced closely in time provided a

finely resolved profile of the protein's sedimentation. A stable plateau was attained for the first few traces (from left to right). In contrast to the equilibrium approach, the high rotor speed rapidly depleted the protein from the center of the rotor, representing the air/solution interface, and formed a boundary that gradually migrated toward the outside of the rotor until a protein pellet formed. The rate at which the boundary moved determined the sedimentation coefficient (s) of CA II, as defined by the Svedberg equation, which states that s equals the ratio of the sedimentation velocity (v) to

the centrifugal field strength (ω^2r). For example, Table 1 summarizes the results obtained from participant 1 who investigated different CA II concentrations and wavelengths in a total of six experiments and deduced an mean average mass of $28,700 \pm 300 \text{ g mol}^{-1}$ by invoking the LAMM data analysis method.

Velocity Time Derivative Analysis

Stafford's dc/dt approach was used to transform sedimentation velocity data into a differential sedimentation coefficient distribution, $g(s^*)$, to provide a more easily interpreted data format, as shown by the gaussian traces in Figure 2E–G. In each case, data collected from multiple scans recorded close together in time were subtracted in pairs and manipulated mathematically. Measured s -values were converted to a standard state of water at 20°C ($s_{20,w}$) using a standard procedure. A single peak was resolved, consistent with a noninteracting monomer and fit to a gaussian function to derive a sedimentation coefficient from the center of the peak and an apparent diffusion coefficient from the width of the peak. Their ratio provided the mass of this species, which was determined to be $28,000 \pm 400 \text{ g mol}^{-1}$ in three independent measurements (Fig. 2E–G). Figure 3C summarizes the velocity-derived sedimentation coefficients generated by three participants who investigated various CA II concentrations and applied different data analysis programs. Results from two participants (2 and 4) were excluded because one reported an outlying value ($s_{20,w} = 3.68$) and the other did not provide any velocity measurements.

Using a combination of equilibrium and velocity approaches and various data analysis methods, native CA II was determined to be a monomer in solution at concentrations relevant to the ITC and SPR portions of the MIRC study. Its molecular mass was deduced to be $29,000 \pm 1,000 \text{ g mol}^{-1}$ from more than 20 independent analyses performed by 5 participants. This value was consistent with the theoretical prediction based on the amino acid sequence ($28,980 \text{ g mol}^{-1}$) and was confirmed experimentally in this study by mass spectrometry (data not shown).

ITC Analysis

Of the 17 groups that volunteered to participate in the ITC portion of the MIRC study, 14 completed the study. Three calorimeter models were employed: CSC 4200 ITC (Calorimetry Sciences Corp., American Fork, UT), MCS-ITC, and VP-ITC (both purchased from MicroCal, LLC, Northampton, MA). Participants were surveyed with respect to the instrumentation used in their laboratories and their experience level. One

group characterized 40–50 macromolecular interactions per year by ITC, while another was beginning to use ITC and had only studied two interactions. Several groups characterized 5–10 biomolecular systems by ITC per year. Participating groups were also experienced in other technologies, including SPR (8 groups), fluorescence (7), AUC (6), circular dichroism (4), NMR (4), differential scanning calorimetry (3), capillary electrophoresis (3), multiple angle light scattering (3), and electrospray mass spectrometry (1).

The goal in designing the ITC study was to assess interlaboratory variability in analyzing a model system with readily measurable K_A and ΔH^{ITC} values. Thus, experimental design was left to the discretion of the ITC participants and varied significantly (Table 2). The array in Figure 4 shows a representative data set collected by each participant, since several submitted multiple data sets. CBS bound CA II in a stoichiometric manner, as indicated by a molar binding ratio (N) of 0.94 ± 0.15 , which was consistent with the reported purity (97% mol) of the CBS sample. The binding reaction was exothermic with an enthalpy change of $\Delta H^{\text{ITC}} = -10.4 \pm 2.5 \text{ kcal mol}^{-1}$ and a binding constant of $K_A = (1.00 \pm 0.22) \times 10^6 \text{ L mol}^{-1}$. Table 3 summarizes the thermodynamic parameters determined by each participant and Figure 5 presents these results as histograms. The influence of experimental factors on the accuracy and precision of the measured binding constants are discussed later in this article.

Accuracy in Determining the Concentration of the Syringe Reactant

For a K_A value that is readily measurable by ITC, the accuracy of all three fitting parameters (N , K_A , and ΔH^{ITC}) is directly proportional to the accuracy with which the syringe reactant (CBS) concentration is determined. In contrast, the accuracy of the cell reactant (CA II) concentration only affects the molar binding ratio (N). In this study, the variability in measuring the concentration of CBS gravimetrically was examined. According to the supplier, the CBS used was 97% mol pure, which is consistent with a mean N value of $0.94 \pm 16\%$ from 14 independent analyses (Fig. 5A). Curve fitting of individual data sets typically yields uncertainties in N of only a few percent, which is consistent with the high precision expected for a well-resolved binding isotherm. For example, the standard errors in N values reported from nonlinear least squares analysis ranged from 0.2 to 5% (excluding participants 10 and 14, who reported errors for replicate measurements). Likewise, the precision in determining ΔH^{ITC} from curve fitting of individual isotherms (standard errors of 0.2 to 7%, excluding participants 10 and 14) was much higher than the

TABLE 2

Instrumentation and Experimental Design Parameters for 14 Isothermal Titration Calorimetry Participants

Participant	Calorimeter	[CBS] ($\mu\text{mol L}^{-1}$)	[CA II] ($\mu\text{mol L}^{-1}$)	μL Test Injection	No. of Injections	μL Injected	Time Interval (s)	Stir Speed (rpm)
1	MCS-ITC	390	16	0	15	10	240	410
2	CSC 4200 ITC	556	71	0	27	10	300	300
3	VP-ITC	400	42	2	31	8	300	310
4	VP-ITC	642	23	0.1	60	4.5	240	300
5	VP-ITC	665	39	1	25	10	240	310
6	VP-ITC	380	37	1	25	10	180	310
7	MCS-ITC	527	52	0	23	10	250	400
8	VP-ITC	198	6.7	1	35	7.5	180	310
9	VP-ITC	1140	56	2	29	5	210	310
10	VP-ITC	384	32	0	30	8	300	310
11	VP-ITC	100	8.6	2	29	10	480	300
12	VP-ITC	896	28	3	39	3	210	300
13	VP-ITC	114	11	1.5	15	18.7	400	300
14	MCS-ITC	300	21	2	19	10	240	400

uncertainty from replicate measurements in the 14 analyses (24%). To assess interlaboratory variation, participants measured and reported the absorbance at $\lambda = 272$ nm of their CBS solution, which enabled us to normalize CBS concentrations across the 14 analyses to within the error of making absorbance measurements. Figure 6 shows a plot of the measured ΔH^{ITC} values as a function of the CBS extinction coefficient calculated from the absorbance and the CBS concentrations reported by each participant. The relatively linear correlation suggests that a significant part of the variability in the reported N , K_A , and ΔH^{ITC} values was due to the variability in determining the concentration of the CBS sample. This observation reinforces the importance of accurately determining the concentration of the syringe reactant and suggests that, when determining parameters using ITC, significant uncertainty exists that is not reflected in the standard errors obtained from nonlinear least squares curve fitting.

Concentration of Cell Reactant Relative to K_A

A second factor related to parameter resolution from ITC isotherms is the total concentration of the reactant in the cell relative to the measured K_A . This relationship has been described by a parameter known as the C-value,¹² which is a dimensionless number equal to the product of the cell reactant concentration (CA II) and the K_A value for its binding interaction with the syringe reactant (CBS). Depending on the signal-to-

noise ratio for a given experiment, C-values between 10 and 100 typically yield reliable K_A values. Higher C-values result in titration curves that are too steep to resolve K_A accurately (although N and ΔH^{ITC} are well resolved) because the cell reactant concentration is too high relative to K_A , whereas lower C-values result in shallow titration curves from which all three parameters (N , K_A , and ΔH^{ITC}) are poorly resolved.

Concentrations of CA II used in the current titrations (7–71 $\mu\text{mol L}^{-1}$) corresponded to C-values ranging from 7 to 75. Figure 7 shows the correlation between the error in K_A determined by curve fitting and the C-value. In general, the K_A values were poorly resolved from experiments performed at C-values near the lower limit (< 20), but resolution did not appear to be compromised for C-values up to the maximum of 75 evaluated in this study. Participant 7 reported an outlying C-value of 55 that resulted in a poorly resolved K_A ; the reason for this is unclear. Data from participants 10 and 14 were excluded from the correlation plot because they reported uncertainties in K_A from replicate determinations (Table 3).

Heats of Mixing

Background heats of mixing are another likely source of error in ITC analysis. Mixing heats are inherent to ITC titrations due to mismatched chemical and temperature environments between the syringe and cell solutions. Moreover, these mixing heats vary according to experimental design parameters, such as the

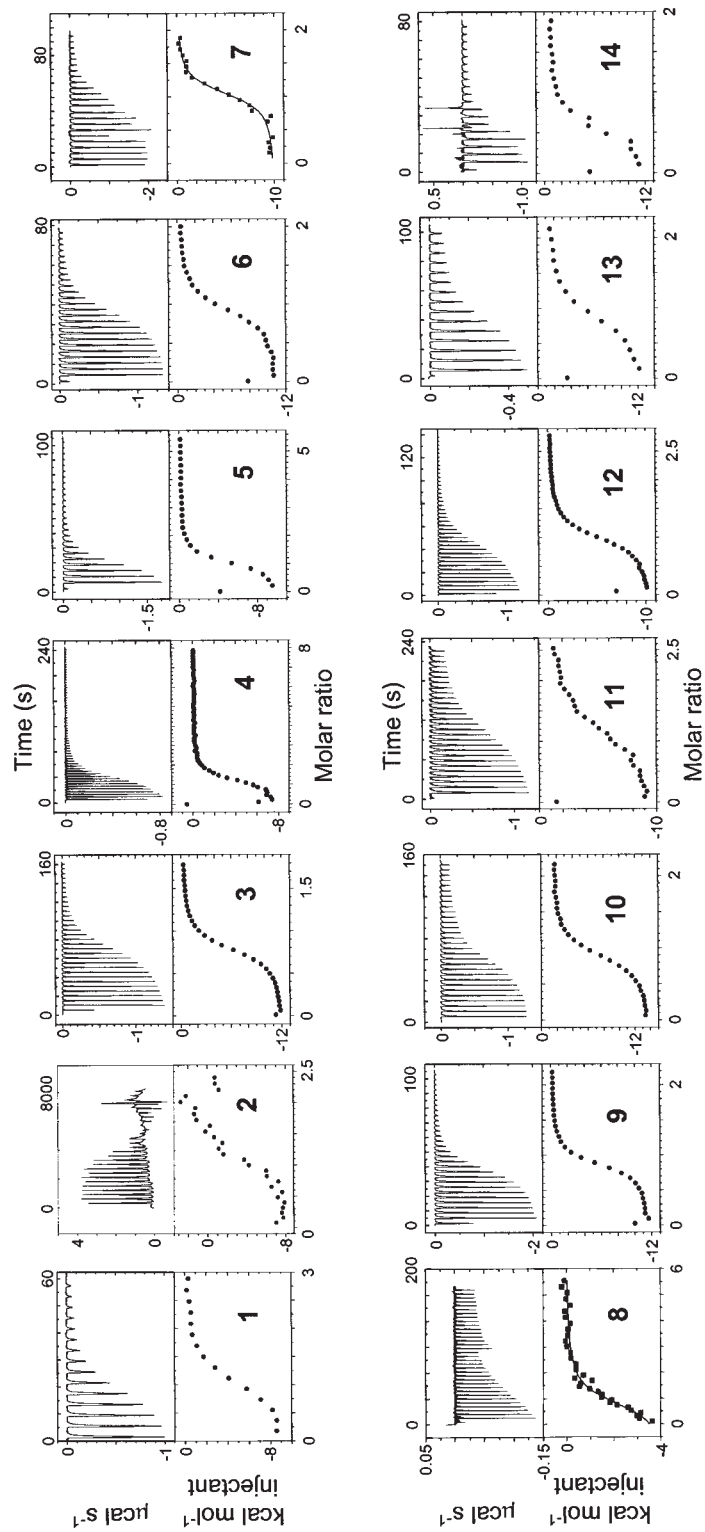
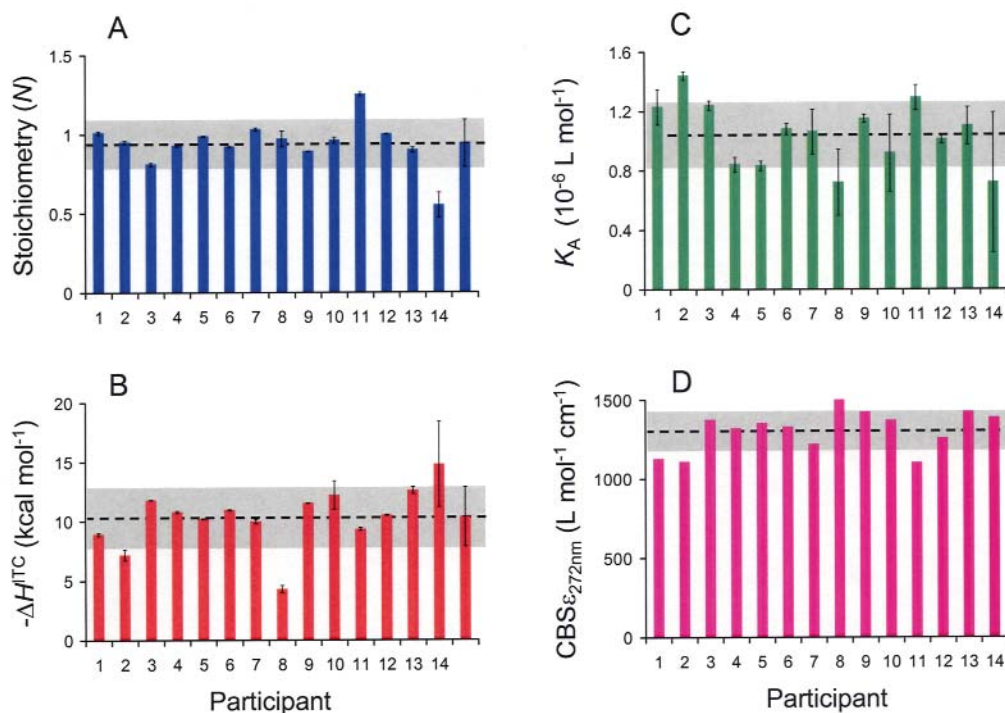
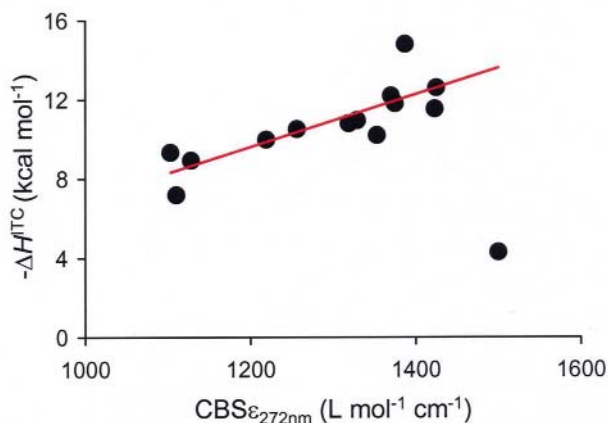


FIGURE 4

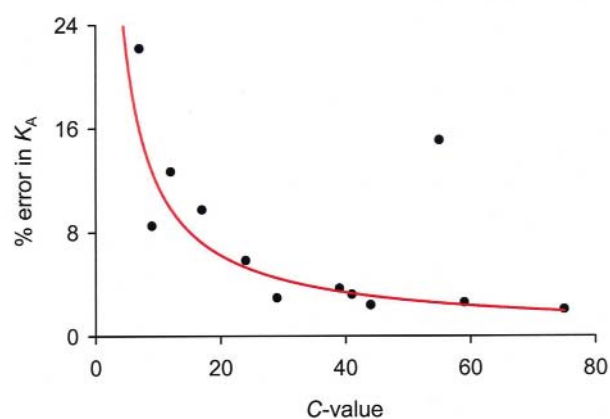
Calorimetric titration data for complex formation between CBS and CA II. For each analysis, *top panels* show the differential power signals recorded for CBS titrations into a cell containing CA II. *Bottom panels* show the same data integrated with respect to time. ΔH_{ITC} , K_A , and N were calculated from nonlinear least-squares analysis using a single-site binding isotherm. Participant numbering correlates with Table 2.

**FIGURE 5**

ITC characterization of the CBS/CA II interaction (based on Fig. 4 and Table 3). **A:** Stoichiometry (0.94 ± 0.15). **B:** Enthalpy upon binding (-10.4 ± 2.5 kcal mol⁻¹). **C:** Affinity [$(1.00 \pm 0.22) \times 10^6$ L mol⁻¹]. **D:** molar extinction coefficient for CBS at 272 nm (1307 ± 126 L mol⁻¹ cm⁻¹). Mean values and the standard deviation for 14 determinations are represented by the horizontal dotted lines and gray bands. Error bars denote the standard deviation of nonlinear least squares analysis, except for participants 10 and 14 who reported standard deviations for replicate analyses. No errors were reported for the extinction coefficient determinations.

**FIGURE 6**

Correlation between the CBS/CA II binding enthalpy change measured by ITC and the calculated molar extinction coefficient for CBS at $\lambda = 272$ nm. The outlying data point at an extinction coefficient value of 1500 L mol⁻¹ cm⁻¹ was excluded from the drawing of the red trend line.

**FIGURE 7**

Correlation between the error in K_A and the C-value for the titration. C-values less than 20 appeared to result in greater uncertainty. The outlying value at a C-value of 70 was excluded from the drawing of the red trend line.

TABLE 3Summary of Reported Isothermal Titration Calorimetry Results^a

Participant	Molar Binding Ratio (<i>N</i>)	K_A ($10^{-6} \times \text{L mol}^{-1}$)	ΔH^{ITC} (kcal mol^{-1})	C-value ^b	Control Titrations
1	1.01 ± 0.01	1.2 ± 0.1	−8.9 ± 0.1	17	CBS into buffer and buffer into CA II. Former subtracted as part of data analysis.
2	0.95 ± 0.01	1.44 ± 0.03	−7.2 ± 0.5	75	None
3	0.81 ± 0.01	1.24 ± 0.03	−11.8 ± 0.02	44	CBS into buffer and buffer into CA II. Former subtracted as part of data analysis.
4	0.929 ± 0.007	0.84 ± 0.05	−10.8 ± 0.1	24	Pilot run.
5	0.987 ± 0.003	0.84 ± 0.03	−10.20 ± 0.04	41	CBS into buffer, subtracted in data analysis.
6	0.921 ± 0.003	1.08 ± 0.04	−10.95 ± 0.05	39	CBS into buffer, subtracted in data analysis.
7	1.03 ± 0.01	1.1 ± 0.2	−10.0 ± 0.2	55	CBS into buffer, subtracted in data analysis.
8	0.97 ± 0.05	0.7 ± 0.2	−4.3 ± 0.3	7.0	CBS into buffer and buffer into CA II. Both subtracted as part of data analysis.
9	0.891 ± 0.002	1.15 ± 0.03	−11.53 ± 0.04	59	CBS into buffer, average value subtracted in analysis.
10 ^c	0.96 ± 0.02	0.9 ± 0.2	−12 ± 1	34	CBS into buffer and buffer into CA II. Average of former used in analysis.
11	1.25 ± 0.01	1.3 ± 0.1	−9.3 ± 0.1	9.0	None
12	1.000 ± 0.003	1.01 ± 0.03	−10.51 ± 0.04	29	Buffer into buffer.
13	0.90 ± 0.02	1.1 ± 0.1	−12.6 ± 0.3	12	CBS into buffer, linear regression subtracted in analysis.
14 ^c	0.55 ± 0.08	0.7 ± 0.3	−15 ± 4	22	CBS into buffer, subtracted in analysis.

^aStandard errors were determined by nonlinear least squares analysis unless noted otherwise.^bC-values were calculated from the mean K_A values.^cParticipants 10 and 14 reported the mean ± standard deviation for three and five titrations, respectively.

injection volume used in the titrations. ITC operators handled the background injection heats with different strategies. Some performed control titrations by injecting CBS into buffer (lacking CA II) and/or injected buffer (lacking CBS) into CA II. Of these, some used one or more of the control titrations to correct the primary titration data of CBS injected into a cell containing CA II. Other participants ignored the background heats, considering them to be a potential source of additional experimental error. If the control heats are sufficiently constant and small over the course of a titration, a constant heat can be subtracted from each titration point so that the heats from each injection (kcal mol^{-1}) are zero at high molar ratios. For example, participant 12 found the background heats to be negligible and consequently excluded the control titration in the analysis, whereas participant 9

conducted a control titration and used the data to correct the primary titration data. Both of these participants employed otherwise similar experimental design parameters and also reported similar binding parameters and uncertainties. It may be that the signal-to-noise ratio for the primary binding data in this study is so much greater than the background heats that correction of the latter was unnecessary. Other cases may not be so favorable. Unfortunately, evaluating whether or not control experiments are required can only be determined empirically.

Additional Experimental Design Variables

Other variations in experimental design included injection volumes (3–18.7 μL), the molar excess of CBS titrated into CA II (8–32 mol CBS per mol of CA II), the

time interval between successive injections (180–480 s), the number of injections (15–60), and the total injection time (60–240 min). None of these appeared to influence parameter accuracy or precision.

SPR Analysis

A study kit and an experimental protocol detailing the SPR portion of the MIRG study were supplied to 70 groups, of which 29 responded. Many participants replicated the analysis, resulting in 60 submitted data sets. All but one data set was collected using BIA-CORE platforms, which comprised S51 (3 data sets/platform), 3000 (27), 2000 (25), 1000 (3), and X systems (1). A single data set was collected using an IASYS biosensor.

Quality Control Test

An often overlooked yet key consideration in planning a biosensor experiment is to use a clean, well-maintained instrument. Prior to interaction analysis, participants were asked to repeatedly inject buffer across a preconditioned but unmodified sensor chip (lacking CA II). This simple experiment provided a suitable quality control test to assess whether the biosensors were functioning properly. Figure 8 depicts 24 example data sets, each showing overlays of 30 replicate buffer responses: These data were processed as outlined in Figure 1. Flat baseline responses were obtained by most participants, as expected, regardless of the platform used. Spikes observed at the injection start and stop times are artifacts that relate to the shift changes resulting from variation in the size of the injection plug as the sample flows in series across the different surfaces. Buffer responses collected early in the run often showed drift that was eliminated over time, emphasizing the stabilizing power of repeatedly injecting buffer. Groups that reported inconsistent buffer injection responses or large deviations in the responses were encouraged to perform extra cleaning or maintenance procedures.

CA II Immobilization

SPR biosensor assays require that one of the reactants be immobilized on the sensor surface. The binding to a second solution-based reactant is then monitored in a label-free and real-time mode. In this study, CA II was covalently immobilized by standard EDC/NHS-mediated amine coupling onto the dextran matrix of a preconditioned and buffer-equilibrated CM5 sensor

chip. Assuming a stoichiometric relationship between reactants in molar terms, the CBS binding response was expected to be at least 150-fold lower than the immobilized level of CA II due to the mass difference between the reacting pair (30,000 g mol⁻¹ and 201.2 g mol⁻¹). To facilitate the detection of small molecules binding to immobilized macromolecular targets, high-capacity surfaces were created. Figure 9 depicts five immobilization profiles that were representative of those obtained by study participants. Different surface capacities were generated when participants deviated from the protocol. The average immobilization level measured for 59 CA II surfaces was 6600 ± 2300 RU.

CBS Binding Profiles

CBS was injected in triplicate at 0, 0.082, 0.25, 0.74, 2.22, 6.67, and 20.0 μmol L⁻¹ across surfaces with and without immobilized CA II. Analyzing a wide concentration series of CBS resulted in a range of binding curves with different shapes, which together provided an information-rich description of the interaction. An example of the CBS/CA II SPR interaction data is shown in Figure 10A. Each 1-min CBS injection provided the “association phase” of complex formation ($t = 0–60$ s). The “dissociation phase” was monitored by washing the surface with buffer for two minutes ($t = 60–180$ s), during which bound CBS was released from immobilized CA II. Since bound CBS dissociated completely from the surface within a minute, no regeneration was required between successive CBS injections.

Raw data were prepared for kinetic analysis as described in Methods. Unmodified flow cells served both as reference and control surfaces to respectively correct for bulk refractive index changes and check for nonspecific binding. Figure 10A demonstrates that the assay was highly reproducible because responses from randomized triplicate CBS injections were superimposable. Binding responses increased in a concentration-dependent manner with respect to CBS concentration and appeared to approach saturation, as evidenced from the plateau responses that coalesced at high CBS concentrations.

Global Analysis of SPR Data

Response data (black lines) shown in Figure 10A were analyzed globally by simulating a set of binding curves (red lines) based on a simple bimolecular reaction mechanism ($A + B = AB$), from which a unique set of association and dissociation rate constants were derived. Their ratio gave an equilibrium dissociation constant ($K_D = k_d/k_a$). The association and dissocia-

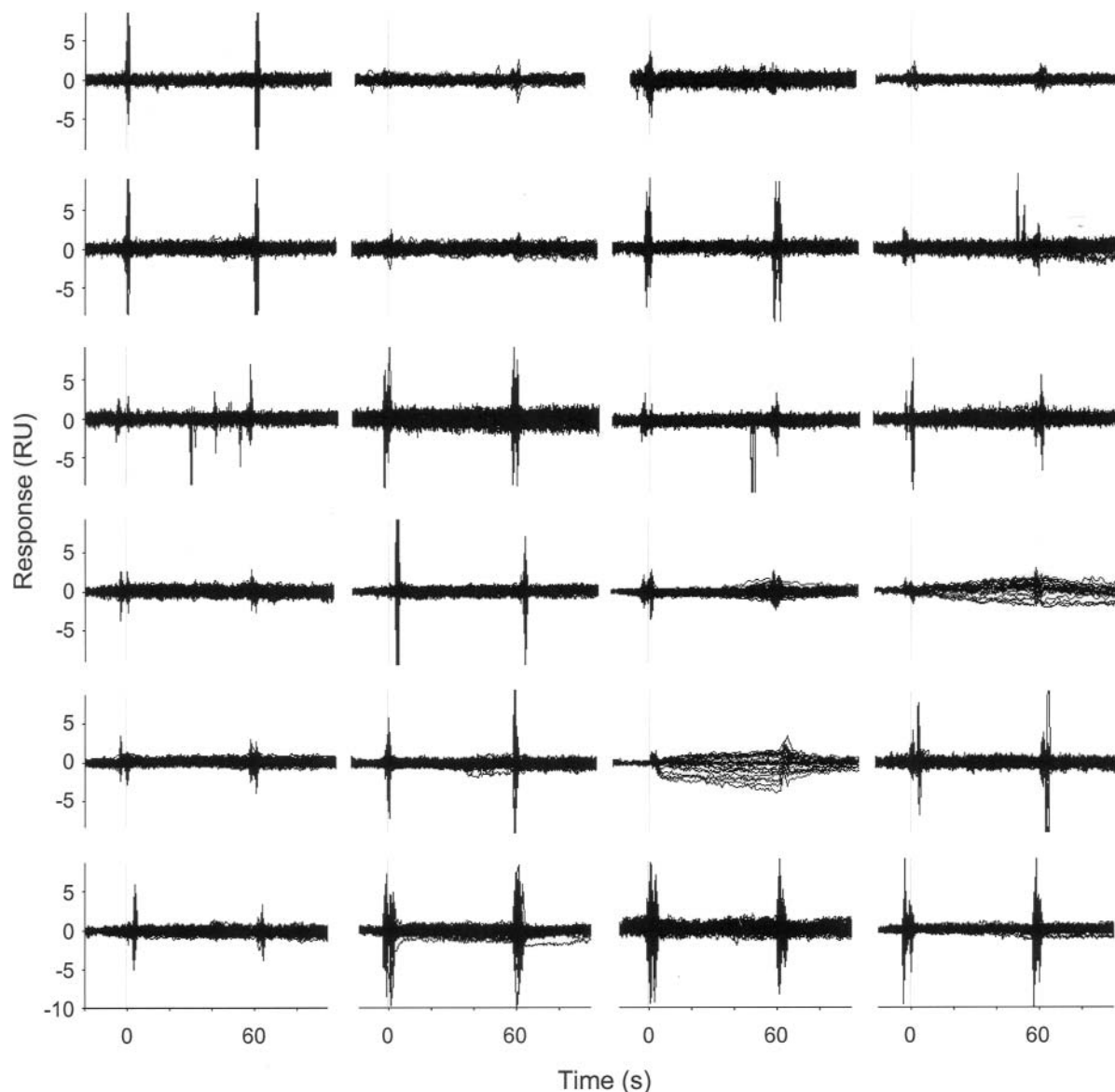


FIGURE 8

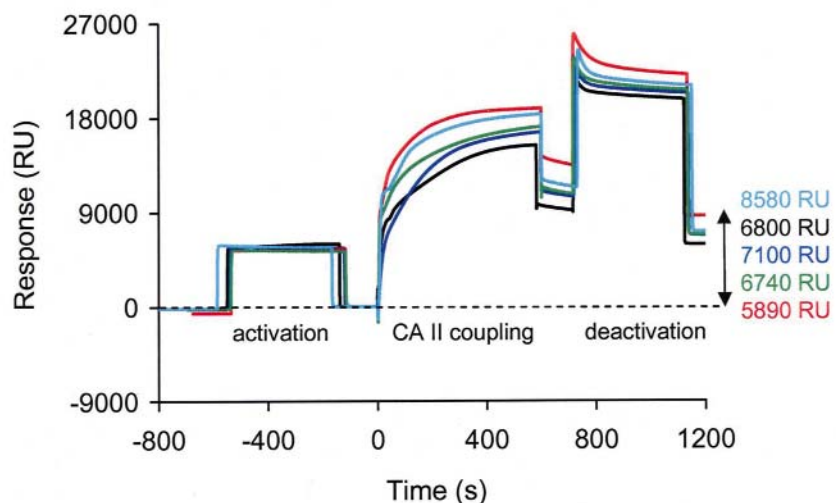
Twenty-four independent analyses of replicate buffer injections across unmodified sensor chips. Data were collected using BIACORE 2000 (three *upper panels*) and 3000 (three *lower panels*) platforms. Each plot shows data from three flow cells; the fourth served as a reference surface.

tion phases of all curves within each data set were fit together to the same reaction model. During the fit, an algorithm samples parameter values iteratively and converges upon an optimal set with minimal residuals. Figure 10B demonstrates the excellent fit that was obtained for this example data set, as indicated by the small difference between the measured and simulated responses (± 1 RU) and their random distribution. This level of scatter is within the acceptable experimental noise for a BIACORE 2000 instrument. In order to

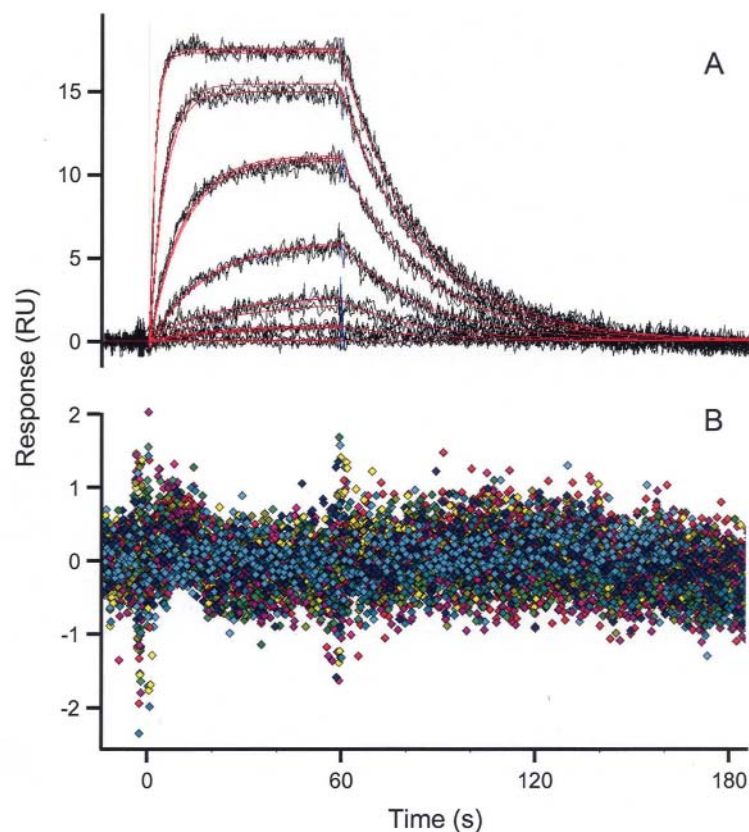
compare the results from the different biosensors and operators, all 60 data sets were processed and fit in the same way. Figure 11 shows an array of all the data sets collected in this study, grouped by instrument type.

Evaluation of Response Data

Inspection of the response data arrayed in Figure 11 showed that all participants acquired kinetically interpretable binding data for a small molecule interaction.

**FIGURE 9**

Examples of five independent CA II immobilization cycles using EDC/NHS-mediated amine coupling (see Methods).

**FIGURE 10**

Global analysis of a typical data set collected on a BIACORE 2000 instrument for CBS binding to immobilized CA II. **A:** Red lines represent data simulated using a simple bimolecular reaction mechanism that were superimposed onto measured responses (black lines). **B:** Residual plot showing the difference between measured and calculated responses.

Measured (black lines) and simulated (red lines) data generally overlaid very well, but the quality of the data varied across the panel due to an interplay of several factors.

High-capacity surfaces typically resulted in data sets that showed systematic drifts, for example 10, 16, 28, and 29, which were generated across 9110, 9220, 8090, and 8830 RU CA II respectively. Other

data sets showed binding responses that were not very reproducible, notably data sets 8, 10, 24, and 28. The cause of this is unclear, but could be due to poor maintenance of these biosensor units.

BIACORE 2000 (data sets 31–55) and 3000 (data sets 4–30) instruments were the most widely used SPR platforms and were well suited to small molecule interaction analysis. Although the short-term noise

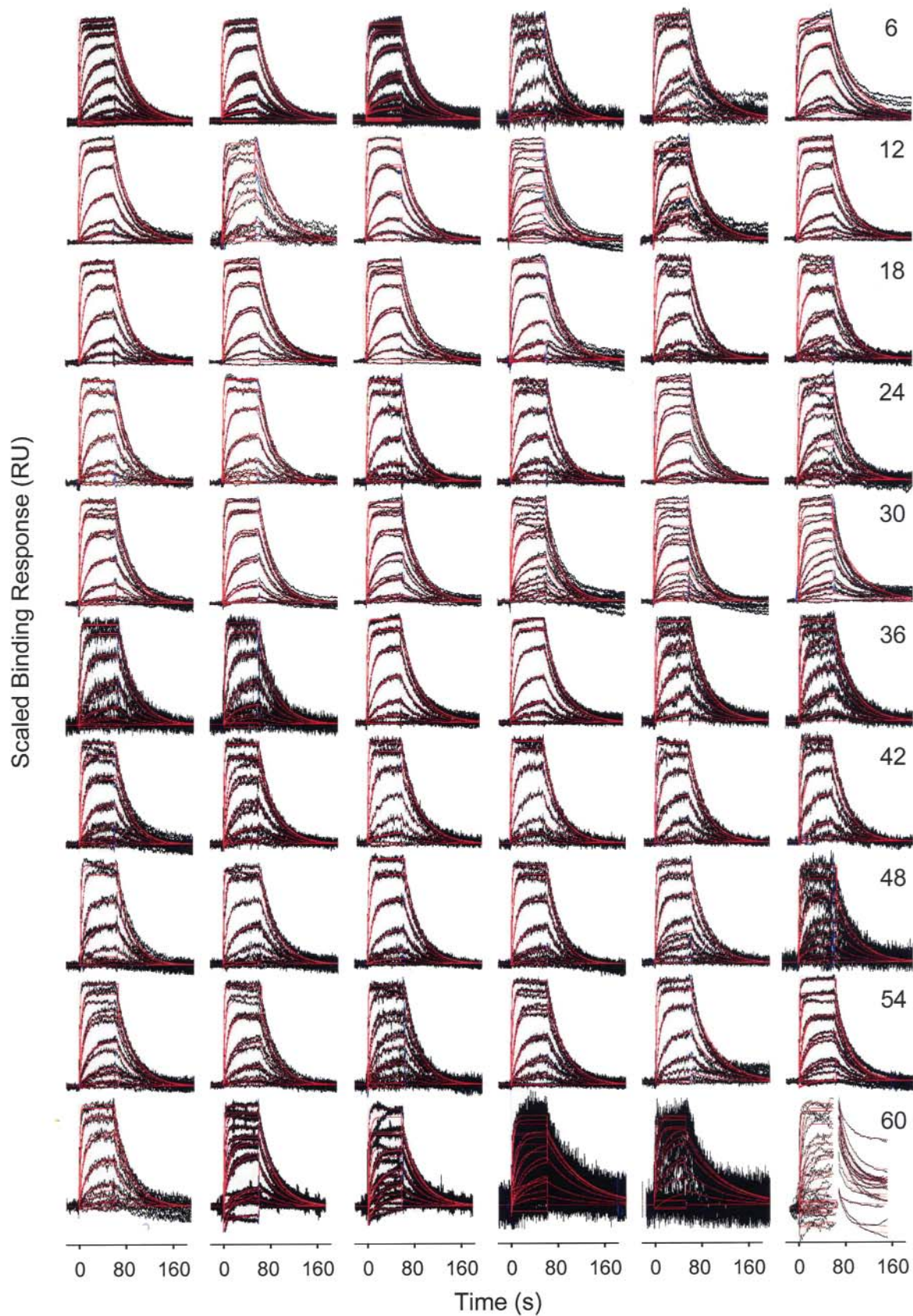


FIGURE 11

Global analysis (red lines) of CBS/CA II binding responses (black lines). Triplicate injections of 0, 0.082, 0.25, 0.74, 2.22, 6.67, and 20.0 $\mu\text{mol L}^{-1}$ CBS were analyzed across differing capacity CA II surfaces. Data were collected on a range of BIACORE systems [S51 (1–3), 3000 (4–30), 2000 (31–55), 1000 (56–58), X (59)] and an IASYS biosensor (60).

level was lower for the 3000 model than the 2000 model, reproducibility in the binding responses was comparable. Since only a single sampling each was obtained from IASYS and BIACORE X, the poor quality of the data could neither be attributed definitively to the instrument nor the operator. Of all biosensor systems tested in this study, BIACORE S51 produced data with the highest signal-to-noise ratio and the highest signal reproducibility (data sets 1–3). This reflects its unique reconfigured flow cell, which has been specifically designed for small molecule applications. In contrast to the serpentine-like configuration offered by earlier BIACORE platforms, the S51 reference and reaction spots lie in the same flow cell, thus providing a closer match between them, increased sensitivity, and a rapid, uniform sample delivery to all spots.

Despite the different noise structures generated by the various biosensor systems, data quality was not compromised with respect to model fitting, as demonstrated by the distributions in the kinetic rate and equilibrium dissociation constants determined across the panel (Figure 12). The average and standard deviation of association and dissociation rate constants were $(4.0 \pm 0.7) \times 10^4 \text{ L mol}^{-1} \text{ s}^{-1}$ and $0.036 \pm 0.007 \text{ s}^{-1}$, respectively, corresponding to an overall binding affinity of $0.90 \pm 0.22 \mu\text{mol L}^{-1}$ for the CBS/CA II binding interaction. The error in each of these parameters was only 20% for the entire panel, which is remarkable given the variability in the systems employed and the experience level of the operators.

Theoretically, a mean immobilized level of $6700 \pm 2200 \text{ RU CA II}$ should result in a binding capacity (or R_{max} value) of approximately 45 RU for an analyte 150-fold lower in molecular mass than the immobilized target, assuming that the latter is 100% active and that the refractive index increments of both reactants are identical. The dotted trend line in Figure 13 represents the theoretical correlation between surface density and capacity, based on these assumptions. The measured surface capacities fell below this line, as shown by the red trend line, suggesting that some of the immobilized protein was inactive. Given that the ITC results implied that the soluble protein was highly active, the loss in binding activity observed by SPR may be attributed to the immobilization process itself. Differences in the refractive index increments of the protein and small molecule cannot, however, be ruled out. As discussed below, any loss in binding capacity did not affect the overall kinetic rate constants or binding affinity.

van't Hoff Analysis

Several groups investigated the influence of temperature on the CBS/CA II interaction by SPR (Fig. 14), to obtain thermodynamic parameters that could be compared with those derived from calorimetry. Figure 14A shows an example of response data (black curves) collected in the same way, but at 5, 15, 25, and 35°C. Global analysis of each data set (red curves) yielded temperature-dependent affinities, which were used to construct van't Hoff plots ($\ln K_D$ vs. $1/T$), as shown in Figure 14B. A van't Hoff enthalpy change of $-10.6 \pm 1.4 \text{ kcal mol}^{-1}$ was computed from the slope (six determinations). A first approximation to the entropy change ($-7.9 \pm 4.4 \text{ cal mol}^{-1} \text{ K}^{-1}$) was given by the Y-axis intercept. Interestingly, this value was very similar to the entropy change ($-7.8 \pm 4.4 \text{ cal mol}^{-1} \text{ K}^{-1}$) calculated by substituting values for the van't Hoff enthalpy change and Gibbs free energy change [$\Delta G^\circ = RT \ln K_D(298 \text{ K})$, where $K_D(298 \text{ K}) = 0.938 \pm 0.18 \mu\text{mol L}^{-1}$] into the Gibbs free energy equation ($\Delta G^\circ = \Delta H_{\text{van't Hoff}} - T\Delta S^\circ$).

DISCUSSION

AUC Summary

AUC confirmed that native CA II molecules were monomers in free solution at concentrations relevant to the ITC and SPR portions of the study. Five independent participants deduced a mean molecular mass of $29 \pm 1 \text{ kg mol}^{-1}$ from complementary equilibrium and velocity approaches, which was consistent with the value determined by mass spectrometry (data not shown) and the theoretical prediction based on amino acid sequence analysis (29.0 kg mol^{-1}). Moreover, the small variability within the multiple (>20) measurements was excellent given the flexibility that was granted to participants regarding their experimental strategies and choice of data analysis method. The AUC results confirmed that CA II was a monomer in solution and supported the use of a simple reaction mechanism to model ITC and SPR data.

ITC Summary

The affinity of the chosen protein/small molecule model system was within a range amenable to ITC and so its determination was not intended to challenge participants. Rather the goal was to obtain a precise solution-based binding affinity for the CBS/CA

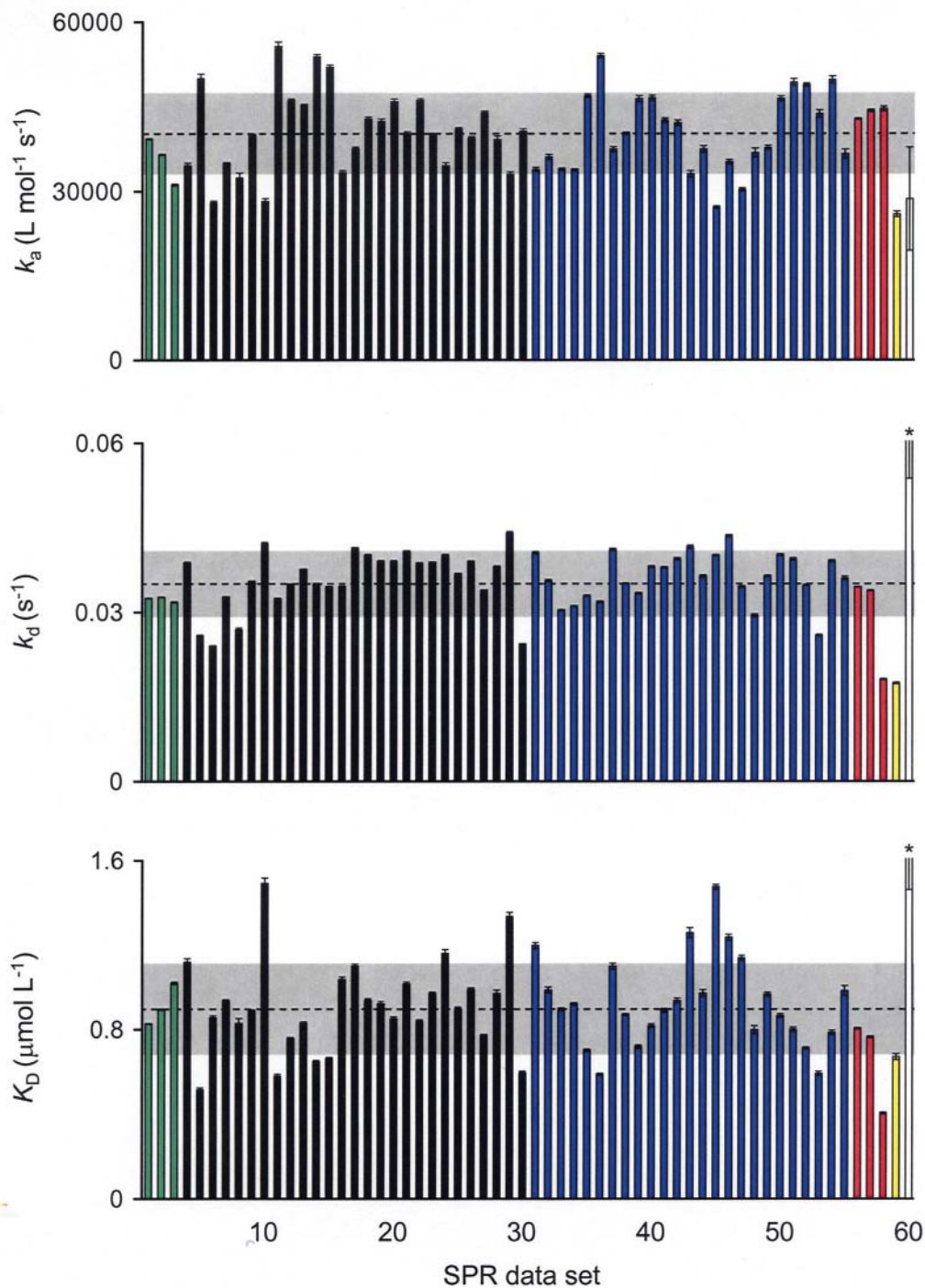
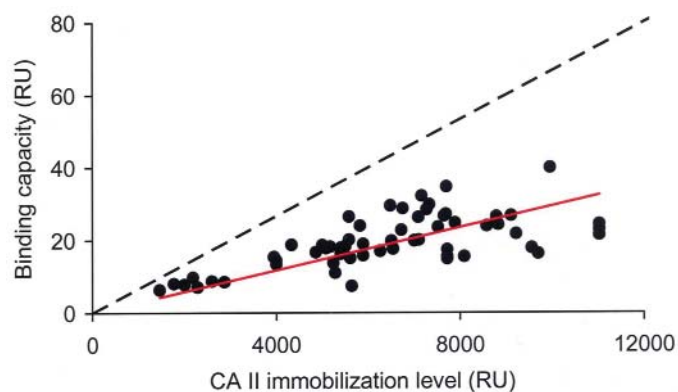
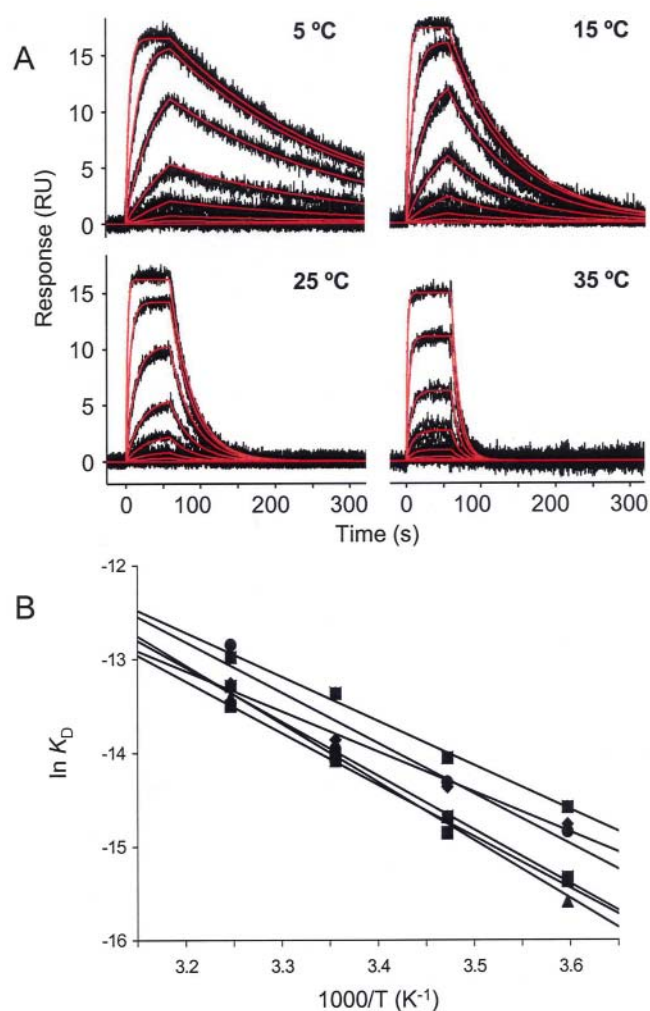


FIGURE 12

Kinetic rate and equilibrium dissociation constants for CBS binding to immobilized CA II (based on Figure 11). Horizontal dotted lines and gray bands represent mean values \pm standard deviations for 59 determinations. Global analysis yielded an affinity of $0.90 \pm 0.22 \mu\text{mol L}^{-1}$ from the kinetic rate constants, $k_a = (4.0 \pm 0.7) \times 10^4 \text{ L mol}^{-1} \text{ s}^{-1}$ and $k_d = 0.036 \pm 0.007 \text{ s}^{-1}$. IASYS data (white bars) were excluded due to an outlying value for k_d ($0.07 \pm 0.01 \text{ s}^{-1}$), which led to a large error in determining affinity ($K_D = 2.3 \pm 0.6 \mu\text{mol L}^{-1}$; truncations are marked by asterisks). BIACORE instruments are color-coded: S51 (green), 3000 (black), 2000 (blue), 1000 (red), and X (yellow).

**FIGURE 13**

Correlation between the level of immobilized CA II and its binding capacity for CBS, as given by the R_{\max} values obtained from data analysis (Fig. 11). The red trend line falls below the dotted line, which represents the theoretical correlation.

**FIGURE 14**

van't Hoff analysis of SPR-derived affinities for the CBS/CA II interaction. **A:** A typical data set showing overlays of globally simulated data (red lines) and measured data (black lines) at various analysis temperatures. **B:** van't Hoff analysis of six affinity determinations at each temperature yielded $\Delta H = -10.6 \pm 1.4 \text{ kcal mol}^{-1}$ from the slope.

II interaction and to assess interlaboratory variation by allowing participants freedom in their experimental design. The precision in determining ΔH^{ITC} (24%) and K_A (22%) and the excellent agreement with our previously reported results¹³ is remarkable given the

variable ways in which the 14 independent titrations were conducted.

As part of the study, participants were invited to raise any issues for discussion. General uncertainties in the accurate determination of the reactant concen-

trations concerned participants. Standard deviations obtained by nonlinear least squares analysis of the best-fit parameters (N , K_A , and ΔH^{ITC}) are misleading because they do not account for the more realistic systematic errors that are associated with determining reactant concentrations, which was addressed in the section above (see Accuracy in Determining the Concentration of the Syringe Reactant).

It was pointed out that the potential unreliability in the first injection reinforces the need for performing a preliminary “test” injection that is excluded from the analysis. For example, titration data obtained from participant 12 (comprising 40 3- μL injections) demonstrated this concern. The reduced size of the initial injection peak compared with subsequent injections was likely the result of decreased concentration of syringe reactant being delivered in the first injection.

The stability of the CA II sample was addressed by two participants. Participant 9 reported that the sample was cloudy after the titration, suggesting that some interlaboratory variability was related to solubility issues. Notably, the titration data for this participant was measured at a CA II concentration of 56 mM, which was twice the average used in this study. A further concern was the use of proper controls to account for background effects, such as heats of mixing. As described above, this was not found to contribute significantly to parameter resolution for the CBS/CA II interaction, given the favorable signal-to-noise ratio.

SPR Summary

While for many of the SPR participants this was the first time that they had attempted to measure the direct binding of a small molecule to an immobilized protein target, it was encouraging to see that all participants returned data sets resembling the expected binding responses. Most of the data sets were described well by a simple interaction model and the resulting binding constants varied by only 20% across the entire panel, which is remarkable considering the variability in instrumental platform and experience level of operators. Numerous participants commented that participation in this study helped raise their level of expertise and that they were interested in participating in future MIRG studies.

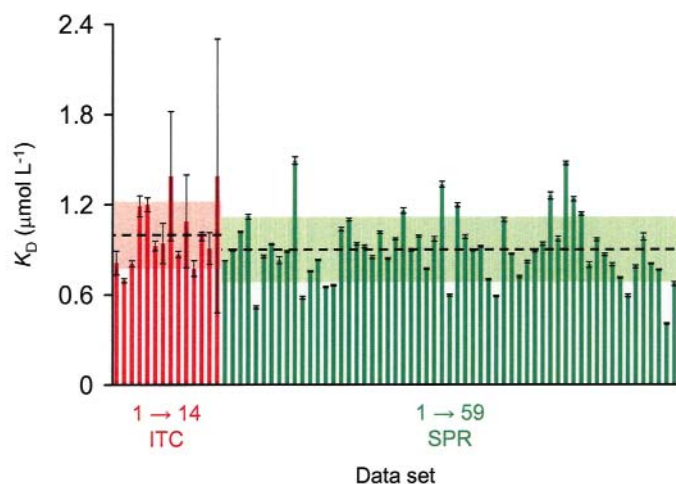
Comparing Solution- and Surface-Based Methods

Since the release of the first commercial biosensor platform in 1990, the results of biosensor analysis

have often been met with skepticism. In part, this has been due to concerns about analyzing macromolecules immobilized onto a surface. Critics have suggested that surfaces significantly alter the binding kinetics, affinity, and thermodynamics of the interactions. By characterizing the same sample using ITC and SPR, the MIRG study provided an opportunity to test whether or not differences were observed between solution- and surface-based measurements. The MIRG study also represented an independent analysis, since most of the participating groups measured the interaction with a single technology. As shown by the distribution of results in Figure 15, the binding affinities obtained for the CBS/CA II interaction by ITC and SPR were within identical experimental error: $K_A^{\text{ITC}} = (1.00 \pm 0.22) \times 10^6 \text{ L mol}^{-1}$ (corresponding to $K_D^{\text{ITC}} = 1.00 \pm 0.22 \mu\text{mol L}^{-1}$) and $K_D^{\text{SPR}} = 0.90 \pm 0.22 \mu\text{mol L}^{-1}$. Taking the analysis a step further, the van't Hoff enthalpy determined by SPR of $-10.6 \pm 1.4 \text{ kcal mol}^{-1}$ was also indistinguishable from the ITC-derived value of $-10.4 \pm 2.5 \text{ kcal mol}^{-1}$ (See Table 4).

The excellent agreement between these enthalpy values suggests that the CBS/CA II binding reaction followed a rigid body mechanism, as described by a two-state transition between bound and unbound molecules. The fact that the thermodynamic parameters (ΔH° and K_D) determined by solution- and surface-based methods matched within experimental error, confirmed that immobilizing the protein on the sensor surface did not modify its binding activity. This is likely because the protein was tethered to the surface via a dextran-based matrix that may maintain some of the entropic freedom of the protein.

The results from this study demonstrate how the corroborative use of three biophysical tools provided a highly resolved and rigorous characterization of a protein/small molecule pair. Table 4 summarizes the final parameter values obtained from this complementary analysis. Inviting a large panel of instrument users to participate in the study tested the competencies of individual researchers and their biophysical tools to analyze the same interaction under universal conditions. Each technique has its advantages and limitations. For example, calorimetry did not impose any molecular weight restriction on reactants, nor was there any signal sensitivity issues due to molecular weight, but the ITC sample consumption was larger than that required by SPR. In contrast, the analysis of small molecules binding to a much larger macromolecular immobilized target is challenging when using SPR, since the phenomenon is influenced by changes in mass at the sensor surface. Discriminating inherently low binding signals from baseline noise, nonspecific

**FIGURE 15**

Comparative ITC- (red) and SPR- (green) derived affinities for the CBS/CA II binding interaction. Horizontal dotted lines and bands indicate affinities of $1.00 \pm 0.22 \mu\text{mol L}^{-1}$ (ITC, $n = 14$) and $0.90 \pm 0.22 \mu\text{mol L}^{-1}$ (SPR, $n = 59$), where standard deviations represent n replicate determinations.

TABLE 4Parameter Summary^a

Parameter	AUC	ITC	SPR
Replicates (n)	>20	14	59 (6 for ΔH°)
MW of CA II (kg mol^{-1}) ^b	29 ± 1	—	—
Stoichiometry (N)	—	0.94 ± 0.15	—
ΔH° (kcal mol^{-1})	—	-10.4 ± 2.5	-10.6 ± 1.4
K_D ($\mu\text{mol L}^{-1}$)	—	1.00 ± 0.22	0.90 ± 0.22
k_a ($\text{L mol}^{-1} \text{s}^{-1}$)	—	—	$(4.0 \pm 0.7) \times 10^4$
k_d (s^{-1})	—	—	0.036 ± 0.007

^aValues represent the mean \pm standard deviation of n replicate determinations.

^bPredicted mass = $28.98 \text{ kg mol}^{-1}$.

binding, and other instrumental artifacts demands careful experimental design and proper data-processing methods.

In conclusion, the similar affinity and thermodynamic results obtained for SPR and ITC by independent groups further validates the use of the biosensor as a biophysical tool. This first MIRC study represents an important step in the creation of validated standards for interaction analysis. In addition, such reagents are valuable teaching tools for new users of established technologies, as well as for the evaluation of new technologies. Both of these areas will undoubtedly expand as our journey to resolve all biomolecular interactions continues.

REFERENCES

1. Perkins SJ. X-ray and neutron scattering analyses of hydration shells: A molecular interpretation based on

sequence predictions and modelling fits. *Biophys Chem* 2001;93:129–139.

2. Johnson ML, Correia JJ, Yphantis DA, Halvorson HR. Analysis of data from the analytical ultracentrifuge by nonlinear least-squares techniques. *Biophys J* 1981;36: 575–588.
3. Stafford WF 3rd. Boundary analysis in sedimentation transport experiments: A procedure for obtaining sedimentation coefficient distributions using the time derivative of the concentration profile. *Anal Biochem* 1992;203:295–301.
4. Philo JS. A method for directly fitting the time derivative of sedimentation velocity data and an alternative algorithm for calculating sedimentation coefficient distribution functions. *Anal Biochem* 2000;279:151–163.
5. Schuck P, Rossmanith P. Determination of the sedimentation coefficient distribution by least-squares boundary modeling. *Biopolymers* 2000;54:328–341.
6. Philo JS. Measuring sedimentation, diffusion, and molecular weights of small molecules by direct fitting of sedimentation velocity concentration profiles. In Schuster TM, Laue TM (eds): *Modern Analytical Ultracentrifugation*, Boston: Birkhauser, 1994:156–170.

7. Behlke J, Ristau O. A new approximate whole boundary solution of the Lamm differential equation for the analysis of sedimentation velocity experiments. *Biophys Chem* 2002;95:59–68.
8. Demeler B, Saber H. Determination of molecular parameters by fitting sedimentation data to finite-element solutions of the Lamm equation. *Biophys J* 1998;74:444–454.
9. Johnsson B, Lofas S, Lindquist G. Immobilization of proteins to a carboxymethyl-dextran-modified gold surface for biospecific interaction analysis in surface plasmon resonance sensors. *Anal Biochem* 1991;198:268–277.
10. Myszka DG. Kinetic, equilibrium, and thermodynamic analysis of macromolecular interactions with BIACORE. *Methods Enzymol* 2000;323:325–340.
11. Myszka DG, Morton TA. CLAMP: A biosensor kinetic data analysis program. *Trends Biochem Sci* 1998;23:149–150.
12. Wiseman T, Williston S, Brandts JF, Lin LN. Rapid measurement of binding constants and heats of binding using a new titration calorimeter. *Anal Biochem* 1989;179:131–137.
13. Day YS, Baird CL, Rich RL, Myszka DG. Direct comparison of binding equilibrium, thermodynamic, and rate constants determined by surface- and solution-based biophysical methods. *Protein Sci* 2002;11:1017–1025.